The Propagation Characteristics of Signal Lines Embedded in a Multilayered Structure in the Presence of a Periodically Perforated Ground Plane

CHI HOU CHAN, MEMBER, IEEE, AND RAJ MITTRA, FELLOW, IEEE

Abstract—**The propagation characteristics of waves along a periodic array of parallel signal lines in a multilayered structure in the presence of a periodically perforated ground plane are studied in this paper. The surface current density on the conductors is expressed in terms of a set of rooftop subdomain basis functions, and Galerkin's procedure is applied to derive a matrix eigenvalue equation for the propagation constant in a numerically efficient manner. The dispersion characteristics of these signal lines are studied for both the balanced and unbalanced excitations with the relative permittivities of the various layers as parameters. Numerical results are presented and compared with available data. Extension of the present method to treat conductors with finite sheet resistances is also included.**

I. INTRODUCTION

PLANAR TRANSMISSION lines play an important role in microelectronic packaging. These transmission lines are in the form of conductive strips, either laid on or embedded in a thin planar dielectric with or without conducting ground planes. The conducting ground planes are often perforated to allow connections of transmission lines located at different separations from the ground planes through a via [1] or because other manufacturing considerations dictate the use of such ground planes.

Analyses of various planar transmission lines have been successfully carried out in the spectral domain by Itoh and Mittra [2] and Itoh [3]. A simplified version of this approach, known as the spectral-domain immittance approach, has been derived by Itoh [4] and employed by several other authors [5], [6]. When the planar transmission lines have constant widths and are infinitely long, the unknown current distribution across the width of the strip can be conveniently expanded in terms of a set of entire domain basis functions. However, when an additional set of orthogonal lines is introduced into the system, or when the ground plane is perforated, the choice of entire domain basis functions is no longer obvious, or even convenient. Recently, waves guided by conductive strips in a mesh-plane environment have been analyzed by Rubin and Bertoni using subdomain basis functions [7], [8].

In [7] and [8], the current distributions on the conducting strips and the ground mesh are expanded in terms of a set of rooftop basis functions and the boundary condition is satisfied in an integral sense by testing the resulting equation with the so-called razor-blade function. Recently, Chan and Mittra [9] have shown that the Galerkin testing procedure provides a more numerically efficient solution than that obtained by using the razor blade.

In contrast to the homogeneously filled transmission lines discussed in [7] and [8], the propagation characteristics of signal lines embedded in a multilayered dielectric medium in the presence of a perforated ground plane are studied in this paper. The multilayered configuration is a more realistic representation of structures used in microelectronic packaging since, typically, the transmission line and the perforated ground plane are supported by a thin dielectric and are separated from other transmission structures by a layer of air or other dielectric. To analyze this structure, the spectral-domain immittance approach is employed to derive the Green's function. The boundary condition is then enforced in conjunction with the Galerkin procedure, leading to an eigenvalue problem which is solved by the Newton–Raphson algorithm. The dispersion characteristic of the structure is calculated for different values of dielectric constants and is compared with results in [7]. Although the present paper also includes discussions on the imperfect conductor case, no numerical results are provided as our primary objective is to study the multilayered effect on the dispersion characteristics.

II. DERIVATION OF THE GREEN'S FUNCTION

The structure considered in this paper is depicted in Fig. 1. The ground plane, located at $y = 0$, is perforated with rectangular apertures; the signal lines are situated at a height t. All conductors are infinitely thin and have a finite sheet resistance R_s. Unlike the structure described in [7], the supporting medium is inhomogeneous and is divided into three stratified regions. Region II is the center

Manuscript received April 10, 1987; revised October 4, 1987.

The authors are with the Electromagnetic Communication Laboratory, Department of Electrical and Computer Engineering, University of Illinois, Urbana, IL 61801.

IEEE Log Number 8820436.

0018-9480/88/0600-0968$01.00 ©1988 IEEE

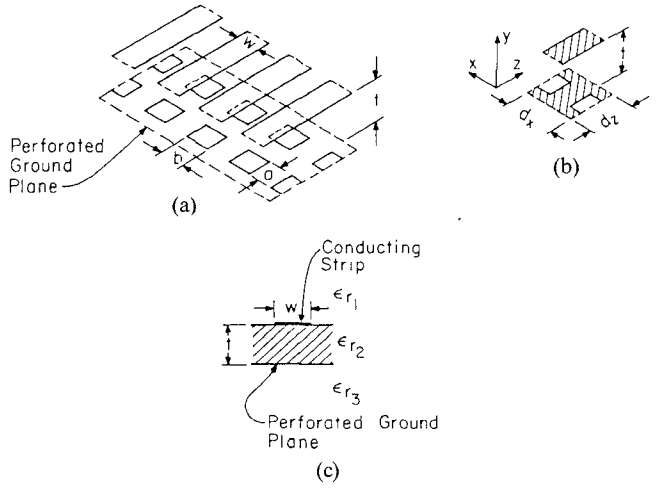

Fig. 1. Array of signal lines above a periodic ground plane supported by a dielectric slab. (a) Isometric view. (b) Unit cell. (c) End view.

region separating the signal lines and the perforated ground plane; regions I and III are the semi-finite regions above the signal lines and below the perforated ground plane, respectively. The spectral Green's function for analyzing this structure can be obtained readily by the spectral-domain immitance approach.

The details of using the spectral-domain immitance approach for deriving the spectral Green's functions of printed transmission lines can be found in [4]; hence, only the final results of the spectral Green's function for the present problem are included.

Following the notations in [4] and denoting the surface current densities on the signal lines and the perforated ground plane as J_x^1 and J_z^1 and J_x^2 and J_z^2, respectively, the relation between the current densities and the transverse (to y) components of the electric field in the spectral domain is given as

$$\begin{bmatrix} \tilde{Z}_{zz}^{11} & \tilde{Z}_{zx}^{11} & \tilde{Z}_{zz}^{12} & \tilde{Z}_{zx}^{12} \\ \tilde{Z}_{xz}^{11} & \tilde{Z}_{xx}^{11} & \tilde{Z}_{xz}^{12} & \tilde{Z}_{xx}^{12} \\ \tilde{Z}_{zz}^{21} & \tilde{Z}_{zx}^{21} & \tilde{Z}_{zz}^{22} & \tilde{Z}_{zx}^{22} \\ \tilde{Z}_{xz}^{21} & \tilde{Z}_{xx}^{21} & \tilde{Z}_{xz}^{22} & Z_{xx}^{22} \end{bmatrix} \begin{bmatrix} \tilde{J}_z^1 \\ \tilde{J}_x^1 \\ \tilde{J}_z^2 \\ \tilde{J}_x^2 \end{bmatrix} = \begin{bmatrix} \tilde{E}_z^1 \\ \tilde{E}_x^1 \\ \tilde{E}_z^2 \\ \tilde{E}_x^2 \end{bmatrix}. \tag{1}$$

The matrix elements are defined as

$$\tilde{Z}_{zz}^{ij} = \left(N_z^2 \tilde{Z}_{ij}^e + N_x^2 \tilde{Z}_{ij}^h\right) \tag{2}$$

$$\tilde{Z}_{xx}^{ij} = \left(N_x^2 \tilde{Z}_{ij}^e + N_z^2 \tilde{Z}_{ij}^h\right) \tag{3}$$

$$\tilde{Z}_{xz}^{ij} = \tilde{Z}_{zx}^{ij} = N_x N_z \left(\tilde{Z}_{ij}^e - \tilde{Z}_{ij}^h\right), \qquad i, j = 1,2. \tag{4}$$

The quantities $\tilde{Z}_{ij}^{e,h}$'s read

$$\tilde{Z}_{11}^{e,h} = \frac{1}{Y_1^{e,h} + Y_{2L}^{e,h}} \tag{5}$$

$$\tilde{Z}_{12}^{e,h} = \frac{1}{Y_3^{e,h} + Y_{2u}^{e,h}} \frac{Y_{\mathrm{TM2,TE2}}/\sinh\gamma_2 t}{Y_1^{e,h} + Y_{\mathrm{TM2,TE2}}\coth\gamma_2 t} \tag{6}$$

$$\tilde{Z}_{21}^{e,h} = \tilde{Z}_{12}^{e,h} \tag{7}$$

$$\tilde{Z}_{22}^{e,h} = \frac{1}{Y_3^{e,h} + Y_{2u}^{e,h}} \tag{8}$$

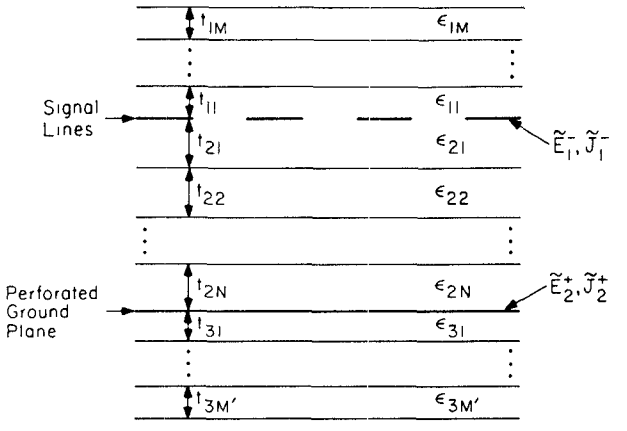

Fig. 2. Signal lines and perforated ground plane embedded in a multilayered dielectric medium.

where

$$Y_1^{e,h} = Y_{\mathrm{TM1,TE1}} \tag{9}$$

$$Y_{2L}^{e,h} = Y_{\mathrm{TM2,TE2}} \frac{Y_{\mathrm{TM2,TE2}} + Y_3^{e,h}\coth\gamma_2 t}{Y_3^{e,h} + Y_{\mathrm{TM2,TE2}}\coth\gamma_2 t} \tag{10}$$

$$Y_3^{e,h} = Y_{\mathrm{TM3,TE3}} \tag{11}$$

$$Y_{2u}^{e,h} = Y_{\mathrm{TM2,TE2}} \frac{Y_{\mathrm{TM2,TE2}} + Y_1^{e,h}\coth\gamma_2 t}{Y_1^{e,h} + Y_{\mathrm{TM2,TE2}}\coth\gamma_2 t} \tag{12}$$

$$Y_{TM_i} = \frac{-j\omega\epsilon_0\epsilon_i}{\gamma_i} \tag{13}$$

$$Y_{\mathrm{TE}i} = \frac{-\gamma_i}{j\omega\mu} \tag{14}$$

$$N_x = \frac{\alpha}{\left(\alpha^2 + \beta^2\right)^{1/2}} \tag{15}$$

$$N_z = \frac{\beta}{\left(\alpha^2 + \beta^2\right)^2} \tag{16}$$

and

$$\gamma_i = \sqrt{\alpha^2 + \beta^2 - \epsilon_i k^2}, \qquad i = 1,2,3. \tag{17}$$

The quantities α and β are the transform variables with respect to the x and z directions, respectively, and will be defined later. The matrix $\tilde{Z}$ is the designated spectral Green's tensor for the present problem. Modifications to include additional stratified layers are readily available using the transfer matrix method described in [10] and [11].

A general structure of signal lines and perforated ground plane embedded in a multilayered structure is depicted in Fig. 2. To include the effects of the dielectric layers both above and below the perforated ground plane, we can follow the procedure discussed in [10] and [11] and modify (9) and (11). The details of this procedure are omitted here; however, the modifications of the spectral Green's tensor due to the presence of the multilayered dielectrics sandwiched between the signal line plane and the perforated ground plane are discussed below in some detail.

We denote the Fourier transform of the tangential scattered electric field and the current densities on the bottom surface of the signal line plane and the top surface of the perforated ground plane by $\tilde{E}_1^-$ and $\tilde{J}_1^-$, and $\tilde{E}_2^+$ and $\tilde{J}_2^+$, respectively. This is illustrated in Fig. 2. Next, we assume that the TE and TM modes have already been decoupled via a coordinate transformation. The subscripts v and u, designating the TM and TE modes as discussed in [4], are suppressed here for simplicity of notation. The tangential scattered electric fields due to the surface current densities are given as

$$\begin{bmatrix} \tilde{E}_2^+ \\ \tilde{J}_2^+ \end{bmatrix} = \prod_{i=1}^{n} [T_i(\gamma_{2i}, t_{2i})] \begin{bmatrix} \tilde{E}_1^- \\ \tilde{J}_1^- \end{bmatrix} \tag{18}$$

where

$$[T_i(\gamma_{21}, t_{21})] = \begin{bmatrix} \cosh\gamma_{2i}t_{2u} & Y_{2i}^{-1}\sinh\gamma_{2i}t_{2i} \\ Y_{2i}\sinh\gamma_{2i}t_{2i} & \cosh\gamma_{2i}t_{2i} \end{bmatrix}. \tag{19}$$

Equation (19) can be rewritten as

$$\begin{bmatrix} \tilde{E}_2^+ \\ \tilde{J}_2^+ \end{bmatrix} = \begin{bmatrix} a_{11} & a_{12} \\ a_{21} & a_{22} \end{bmatrix} \begin{bmatrix} \tilde{E}_1^- \\ \tilde{J}_1^- \end{bmatrix} \tag{20}$$

or

$$\begin{bmatrix} \tilde{E}_1^- \\ \tilde{J}_1^- \end{bmatrix} = \begin{bmatrix} a_{11} & a_{12} \\ a_{21} & a_{22} \end{bmatrix}^{-1} = \begin{bmatrix} b_{11} & b_{12} \\ b_{21} & b_{22} \end{bmatrix} \begin{bmatrix} \tilde{E}_2^+ \\ \tilde{J}_2^+ \end{bmatrix}. \tag{21}$$

The boundary conditions governing (20) and (21) read

$$\tilde{E}^+ = \tilde{E}^- = \tilde{E} \tag{22}$$

$$\tilde{J}^+ = Y^+\tilde{E} \tag{23}$$

and

$$\tilde{J}^- = -Y^-\tilde{E}. \tag{24}$$

After some simple manipulations, one obtains

$$\begin{bmatrix} \tilde{E}_1 \\ \tilde{E}_2 \end{bmatrix} = \begin{bmatrix} Y_1^+ - \dfrac{b_{22}}{b_{12}} & -b_{21} + \dfrac{b_{22}b_{11}}{b_{12}} \\ a_{21} - \dfrac{a_{11}a_{22}}{a_{12}} & \dfrac{a_{22}}{a_{12}} + Y_2^- \end{bmatrix}^{-1} \begin{bmatrix} \tilde{J}_1 \\ \tilde{J}_2 \end{bmatrix} = \begin{bmatrix} c_{11} & c_{12} \\ c_{21} & c_{22} \end{bmatrix} \begin{bmatrix} \tilde{J}_1 \\ \tilde{J}_2 \end{bmatrix}. \tag{25}$$

Y_1^+ and Y_2^- are the input admittances looking upward from the signal lines and downward from the perforated ground plane in an equivalent transmission line model, respectively. These quantities can be constructed easily following the procedures discussed in [10] and [11]. Although the two off-diagonal terms in (25) take a different form, it can be shown that they are nontheless equivalent.

To include the effects of the dielectric layers between the signal line plane and the perforated ground plane, (5) to (8) are replaced by

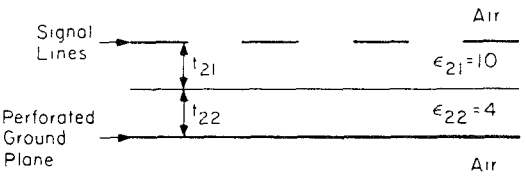

Fig. 3. Signal lines and perforated ground plane supported by two layers of dielectrics

$$\begin{bmatrix} Z_{11}^{e,h} & Z_{12}^{e,h} \\ Z_{21}^{e,h} & Z_{22}^{e,h} \end{bmatrix} = \begin{bmatrix} C_{11} & C_{12} \\ C_{21} & C_{22} \end{bmatrix} \tag{26}$$

with Y_1^+, Y_2^-, and Y_{2i} replaced by $Y_{\mathrm{TM1,TE1}}^+$, $Y_{\mathrm{TM2,TE2}}^+$, and $Y_{\mathrm{TM2}i,\mathrm{TE2}i}$, respectively. Using the coordinate transformation given in (2) to (4), a matrix equation similar to (1) for a general multilayered structure can be obtained. If the number of dielectric layers between the signal line plane and the perforated ground plane is small, e.g., one or two, we can derive analytical expressions for the elements of the matrix in (26). As an example, we present below the expressions for the elements of the Green's tensor for the structure shown in Fig. 3.

The above structure has two dielectric layers between the signal line plane and the perforated ground plane. The Green's function tensor is very similar to the one for the structure shown in Fig. 1 except that the quantities $Y_{2L}^{e,h}$ and $Y_{2u}^{e,h}$ are replaced by

$$Y_{2L}^{e,h} = Y_{\mathrm{TM21,TE21}} \frac{Y_3^{e,h}C_1 + Y_{\mathrm{TM22,TE22}}C_2}{Y_3^{e,h} + Y_{\mathrm{TM22,TE22}}C_2} \tag{27}$$

and

$$Y_{2u}^{e,h} = Y_{\mathrm{TM22,TE22}} \frac{Y_1^{e,h}C_3 + Y_{\mathrm{TM21,TE21}}C_2}{Y_1^{e,h} + Y_{\mathrm{TM21,TE21}}C_1} \tag{28}$$

where

$$C_1 = \frac{Y_{\mathrm{TM21,TE21}} + Y_{22}^{e,h}\coth\gamma_{21}t_{21}}{Y_{21}^{e,h} + Y_{22}^{e,h}} \tag{29}$$

$$C_2 = \frac{Y_{\mathrm{TM21,TE21}}\coth\gamma_{22}t_{22} + Y_{\mathrm{TM22,TE22}}\coth\gamma_{21}t_{21}}{Y_{21}^{e,h} + Y_{22}^{e,h}} \tag{30}$$

$$C_3 = \frac{Y_{\mathrm{TM22,TE22}} + Y_{21}^{e,h}\coth\gamma_{22}t_{22}}{Y_{22}^{e,h} + Y_{21}^{e,h}} \tag{31}$$

$$Y_{21}^{e,h} = Y_{\mathrm{TM21,TE21}}\coth\gamma_{21}t_{21} \tag{32}$$

and

$$Y_{22}^{e,h} = Y_{\mathrm{TM22,TE22}}\coth\gamma_{22}t_{22}. \tag{33}$$

The Green's function tensor can be generated numerically using (19), (20), and (25) when the number of dielectrics between the signal line plane and the perforated ground plane exceeds two layers.

III. Formulation of the Eigenvalue Problem

In general, the current distribution on a periodic structure shown in Fig. 1 is not periodic unless the excitation is also periodic. For example, if we assume that all the currents on the strips are identical and that they flow in the same direction (unbalanced excitation), we can insert a magnetic wall midway between two adjacent strips without disturbing the fields. Alternatively, if the excitation is such that the currents on two adjacent strips flow in opposite directions (balanced excitation), an electric wall can be inserted between the strips without disturbing the fields. Under these excitation conditions, we can identify a unit cell, as depicted in Fig. 1(b), for the structure under investigation. The periodicities of the unit cell in the x and z directions are denoted by d_x and d_z, respectively. The Fourier transform variables α and β are then defined as

$$\alpha = \frac{2\pi m}{d_x} = m\,\Delta\alpha \tag{34}$$

and

$$\beta = \frac{2\pi n}{d_z} + k_z = n\,\Delta\beta + k_z \tag{35}$$

where k_z is the propagation constant of the signal line.

The current density $\vec{J}_s$ within the unit cell is approximated as a linear combination of x- and z-directed rooftop functions. The details of this discretization procedure can be found in [7]–[9] and will be omitted here. The transverse component of the electric field $\vec{E}_t$ is expressed in terms of the current density $\vec{J}_s$ by the inverse Fourier transform given by (1). The electric field boundary condition on the unit cell that includes both the signal line and the perforated ground plane reads

$$\vec{E}_t - R_s\vec{J}_s = 0. \tag{36}$$

Denoting the complex current coefficients of the rooftop functions as $I^{1,2}_{x,z}$ and applying the Galerkin procedure, we obtain a determinantal equation which reads

$$\begin{bmatrix} G^{11}_{zz} & G^{11}_{zx} & G^{12}_{zz} & G^{12}_{zx} \\ G^{11}_{xz} & G^{11}_{xx} & G^{12}_{xz} & G^{12}_{xx} \\ G^{21}_{zz} & G^{21}_{zx} & G^{22}_{zz} & G^{22}_{zx} \\ G^{21}_{xz} & G^{21}_{xx} & G^{22}_{xz} & G^{22}_{xx} \end{bmatrix} \begin{bmatrix} I^1_z \\ I^1_x \\ I^2_z \\ I^2_x \end{bmatrix} = \begin{bmatrix} 0 \\ 0 \\ 0 \\ 0 \end{bmatrix}. \tag{37}$$

Each of the G's is a submatrix which contains the following elements:

$$G^{IJ}_{pq}(k,l) = \sum_{m=-\infty}^{\infty}\sum_{n=-\infty}^{\infty} \tilde{Z}^{IJ}_{pq}\tilde{R}_q\tilde{R}^*_p e^{-j[\alpha(x^k_p - x^l_q)+\beta(z^k_p - z^l_q)]} + R_s F^{kl}_{pq} \tag{38}$$

$$F^{kl}_{pq} = \begin{cases} \int R^k_q R^{p'}\,ds, & I = J = 1,2;\ p = q = x, z \\ 0; & \text{otherwise.} \end{cases} \tag{39}$$

$\tilde{R}_q$ denotes the Fourier transform of a q-directed rooftop function centered at the origin whereas R^l_q denotes a q-directed rooftop function centered at x^l_q and z^l_q. As we will discuss in the next section, R_q can also represent a half-rooftop function. The expression for F^{kl}_{pq}, obtained after carrying out the integral in (39), can be found in [9] and is omitted here.

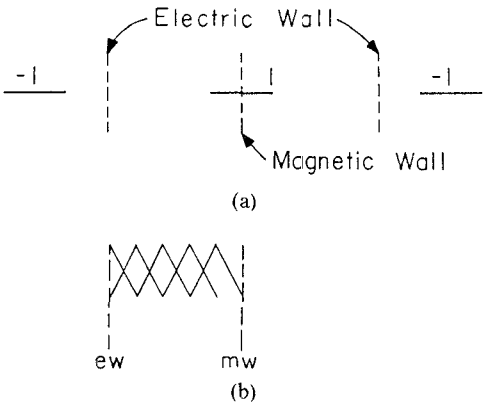

Fig. 4. Signal lines under balanced excitation. (a) Unit cell. (b) Current representation for J_x in the x direction.

The doubly infinite summation, which appears in (38), has the following asymptotic behavior: for $I = J$,

$$\frac{1}{m^2n^2(m^2+n^2)^{1/2}} \tag{40}$$

however, if the razor blade testing function [7] is used, we have

$$\frac{1}{mn(m^2+n^2)^{1/2}}. \tag{41}$$

When $I \neq J$, both (40) and (41) are multiplied with an extra decaying factor of $1/\sinh(\gamma_2 t)$. These asymptotic behaviors indicate that the doubly infinite summation converges much more rapidly when the Galerkin testing procedure is used in place of razor blade testing. The unknown k_z in the determinantal equation in (37) is solved iteratively using the Newton–Raphson procedure. For each iteration, the matrix elements are calculated anew. As a result, a significant reduction in computer time can be achieved by using the Galerkin testing procedure. Further reduction can be obtained by a summation technique using the fast Fourier transform (FFT) algorithm. This technique has been discussed in [9] and is omitted here.

IV. Balanced and Unbalanced Excitations of the Signal Lines

As mentioned earlier, excitations on the signal lines determine the choice of electric or magnetic walls that can be inserted midway between two adjacent lines without disturbing the fields. Fig. 4(a) depicts a balanced excitation on which the unit cell has two electric sidewalls. The x-directed current elements are nonzero at the electric walls. Furthermore, by invoking symmetry, a magnetic wall can be inserted midway between the two electric walls. The x-directed current elements, however, are zero

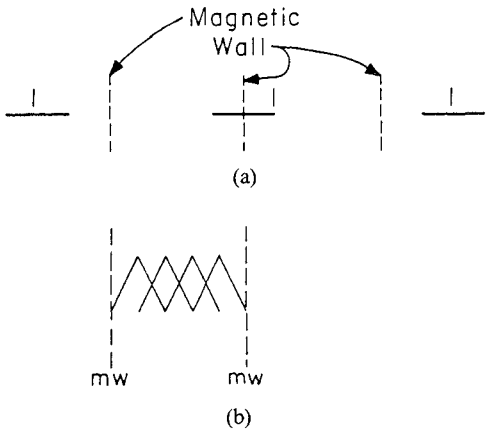

Fig. 5. Signal lines under unbalanced excitation (a) Unit cell. (b) Current representation for J_x in the x direction.

at the magnetic wall. Thus, the right half of a rooftop function, as show in Fig. 4(b), must be used to correctly represent the current density J_x. For an unbalanced excitation, the electric walls are replaced by the magnetic ones.

Fig. 5(a) depicts the unit cell with magnetic sidewalls under unbalanced excitation and Fig. 5(b) shows the current representation for J_x. In both the balanced and unbalanced excitations, J_z are continuous and not necessarily zero at the boundaries of the unit cell in the z direction; hence they are represented by half-rooftop functions. However, due to the periodicity in the z direction, the two half-rooftop functions at the two boundaries have equal amplitudes and a phase shift of $e^{-j\beta d_z}$. As a result, these two half-rooftop functions can be combined to form a single rooftop [7].

Side-by-side coupling between two adjacent signal lines is also investigated in this paper. Fig. 6 shows the geometry of a pair of coupled lines, derived by removing every third line of the structure in Fig. 1. Again, we limit our discussion to the balanced and unbalanced excitations. For the balanced case, the unit cell is enclosed by two electric side walls. The current flowing in the two signal lines within the unit cell are equal in magnitude and opposite in direction. As a result, an electric wall can be introduced midway between the two signal lines; hence, the problem is reduced to that of solving a single line enclosed by two electric walls with a slight modification on the matrix elements in (37). Similarly, for the unbalanced excitation, the problem reduces to a single line enclosed by two magnetic walls.

In order to modify the matrix elements in (37) that account for the even and odd symmetries of the structures, we first study the matrix equation in (1). The amplitudes of the current elements are either evenly symmetric or oddly symmetric about the $y-z$ plane. As a result, the matrix can be reduced to one quarter of its original size by invoking these symmetries. Furthermore, it can be shown that when $p \neq q$, the element Z_{pq}^{IJ} has an odd symmetry about $\alpha = 0$ in the spectral domain; otherwise, it has an even symmetry. In view of this, the doubly infinite summation appearing in (38) for calculating the matrix element

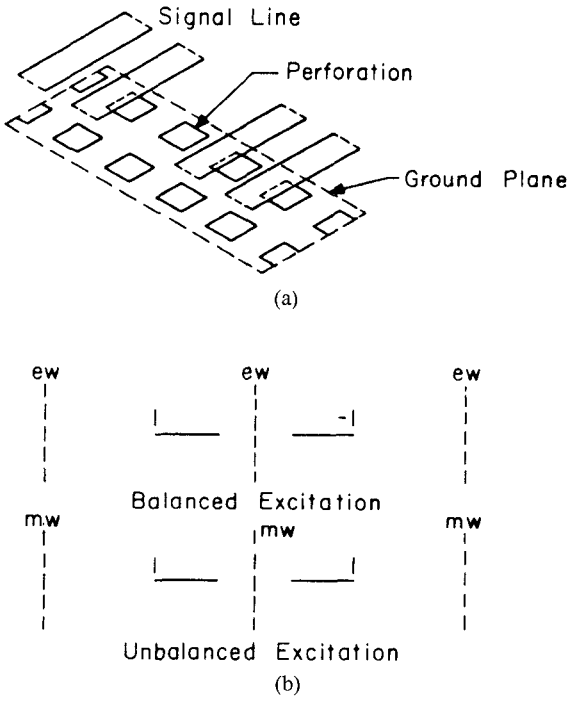

Fig. 6. Side-by-side coupled signal line. (a) Isometric view. (b) Unit cell with appropriate boundary conditions.

G_{pq}^{IJ} can be rewritten as

$$4\Delta\alpha\Delta\beta \sum_{n=-\infty}^{\infty} \left\{ \frac{1}{2} \tilde{Z}_{pq}^{IJ} f_1(\alpha) \tilde{R}_p^* e^{-j\alpha x_p^k} \Big|_{\alpha=0} + \sum_{m=1}^{\infty} Z_{pq}^{IJ} f_1(\alpha) f_2(\alpha) \right\} e^{-j\beta(z_p^k - z_q^l)} \quad (42)$$

where

$$f_1(\alpha x) = \begin{cases} \text{Real} \left\{ \tilde{R}_q e^{j\alpha x_q^l} \right\} & \text{even symmetry} \\ j \text{ Imaginary} \left\{ \tilde{R}_q e^{j\alpha x_q^l} \right\} & \text{odd symmetry} \end{cases} \quad (43)$$

and

$$f_2(\alpha x) = \begin{cases} \text{Real} \left\{ R_p^* e^{j\alpha x_p^k} \right\} \\ \qquad \text{even symmetry, } p = q; \\ \qquad \text{or odd symmetry, } p \neq q \\ j \text{ Imaginary} \left\{ \tilde{R}_p^* e^{-j\alpha x_p^k} \right\} \\ \qquad \text{even symmetry, } p \neq q; \\ \qquad \text{or odd symmetry, } p = q. \end{cases} \quad (44)$$

The determinantal equation of (37) may be solved either by using the modified matrix elements given in (42) or by working with the expressions for these elements in their original forms. When symmetry of the structure is invoked, the matrix size is reduced to about one-fourth of its original size, although more CPU time is needed to evaluate the matrix elements. On a vector machine, e.g., the Cray X-MP/48, it is faster to solve the eigenvalue problem without invoking the symmetry of the structure. This is due to the fact that once the symmetry is invoked, the

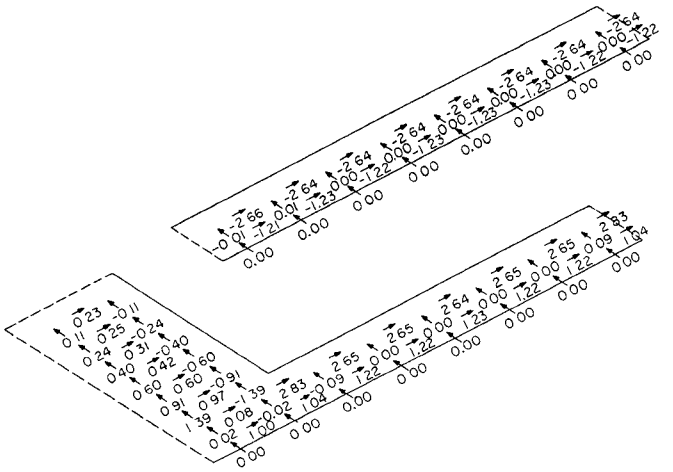

Fig. 7. Current distribution in the signal line and the ground plane over half of the unit cell of the structure shown in Fig. 1 under unbalanced excitation. ($R_s = 0$, $w = 0.25$ cm, $a = b = 0.75$ cm, $d_1 = d_2 = 1.0$ cm, $k_0 = 0.0001$ cm^{-1}, $N = 8$, $M = 16$, $\epsilon_{r1} = \epsilon_{r2} = \epsilon_{r3} = 1$.)

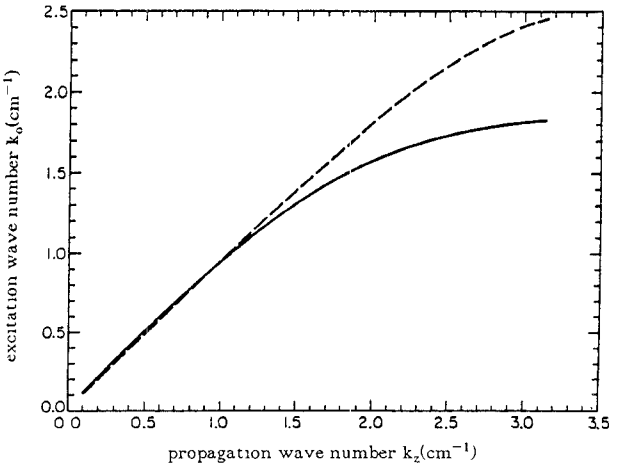

Fig. 8. Dispersion characteristics of the structure shown in Fig. 1. ---- balanced excitation; —— unbalanced excitation. ($R_s = 0$, $w = 0.25$ cm, $a = b = 0.75$ cm, $d_1 = d_2 = 1.0$ cm, $N = 8$, $M = 16$, $\epsilon_{r1} = \epsilon_{r2} = \epsilon_{r3} = 1$.)

computer code to evaluate the matrix elements is not vectorizable and, hence, required a longer execution time.

The dispersion characteristics of signal lines over a perforated ground plane in a multilayered medium are presented in the next section.

V. Numerical Results

The eigenvalue problem of (37) is solved by the Newton–Raphson iteration procedure. The criteria to terminate the iteration procedure are the same as those adopted in [7]. The doubly infinite series appearing in (38) and (42), as consequences of the Galerkin testing procedure, are truncated according to

$$N = \frac{d_z}{\Delta z} \qquad M = \frac{d_x}{2\Delta x} \tag{45}$$

as opposed to $M = d_x/\Delta x$ used in [7] when the razor blade testing is used. To examine the effect of the testing function on the eigenvalue solution, we first consider the effect on the current distribution by using the Galerkin testing procedure as opposed to the razor blade testing.

Fig. 7 shows the current distribution in the structure of Fig. 1 under unbalanced excitation when the Galerkin testing procedure is employed. In general, the surface current density follows a distribution similar to the one shown in [7, fig. 5], where razor blade testing is used.

Fig. 8 shows the dispersion characteristics of the structure shown in Fig. 1 with all the dielectric constants equal to unity. For k_0 less than 1 cm^{-1}, the balanced and unbalanced modes have similar propagation constants and are both close to the TEM mode propagation. When k_0 is greater than 1 cm^{-1}, the balanced and unbalanced modes begin to have different dispersion characteristics and eventually cut off at different wavenumbers.

Fig. 9 shows the dispersion characteristics of the structure in Fig. 1 with $\epsilon_1 = \epsilon_3 = 1$ and $\epsilon_2 = 10$. Both the balanced and unbalanced modes are very different from the TEM mode propagation for k_0 greater than 0.1. The two

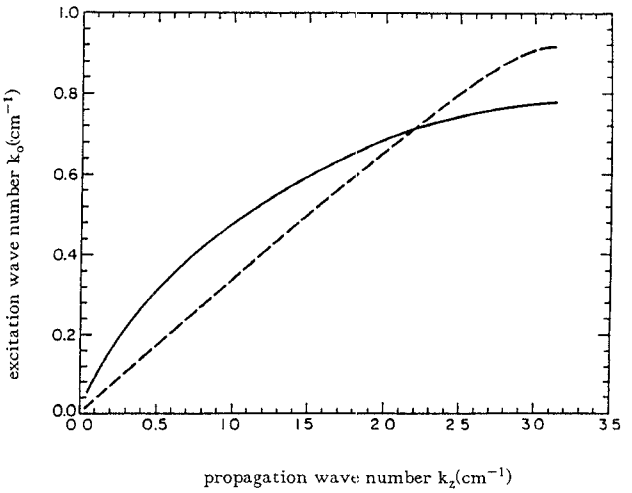

Fig. 9. Dispersion characteristics of the structure shown in Fig. 1. ---- balanced excitation; —— unbalanced excitation. ($R_s = 0$, $w = 0.25$ cm, $a = b = 0.75$ cm, $d_1 = d_2 = 1.0$ cm, $N = 8$, $M = 16$, $\epsilon_{r1} = \epsilon_{r3} = 1$, $\epsilon_{r2} = 10$.)

dispersion curves intersect at about $k_0 = 0.7$ cm^{-1}. The cutoff wavenumbers of both modes are much lower than those when the dielectric is replaced by air.

The structure shown in Fig. 1, with $\epsilon_1 = \epsilon_2 = \epsilon_3 = 1$ and every other signal line removed, has been studied by Rubin and Bertoni [7] and the dispersion characteristic has been shown in [7, fig. 8]. Apparently, the scale of the ordinate axis in that figure is incorrect between $k_0 = 2$, and 3. Instead of reproducing the dispersion curve for the same structure, Fig. 10 shows the dispersion characteristic for $\epsilon_2 = 10$. Both the balanced and unbalanced modes are very different from the TEM propagation at the frequency range of interest.

Fig. 11 shows the dispersion characteristic of the structure shown in Fig. 3. This structure consists of two dielectric layers with $\epsilon_{21} = 10$ and $\epsilon_{22} = 4$ while the total thickness of the dielectric regions remains the same as in the structure shown in Fig. 1. We observe that the cutoff

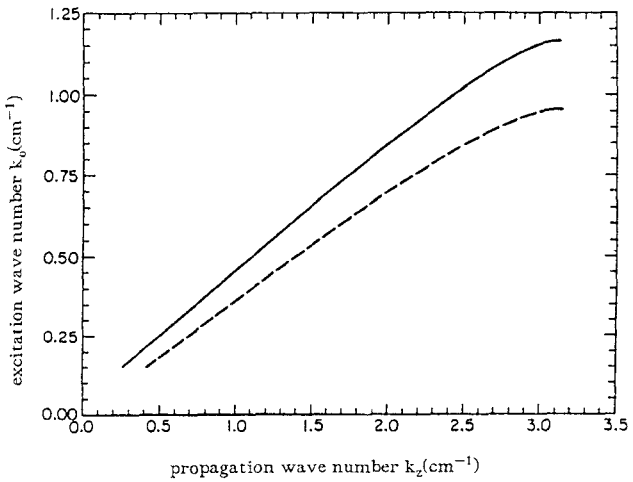

Fig. 10. Dispersion characteristics of the structure shown in Fig. 1 with every other line removed. ---- balanced excitation; —— unbalanced excitation. ($R_s = 0$, $w = 0.25$ cm, $a = b = 0.75$ cm, $d_1 = 1.0$ cm, $d_2 = 2.0$ cm, $N = 8$, $M = 32$, $\epsilon_{r1} = \epsilon_{r3} = 1$, $\epsilon_{r2} = 10$.)

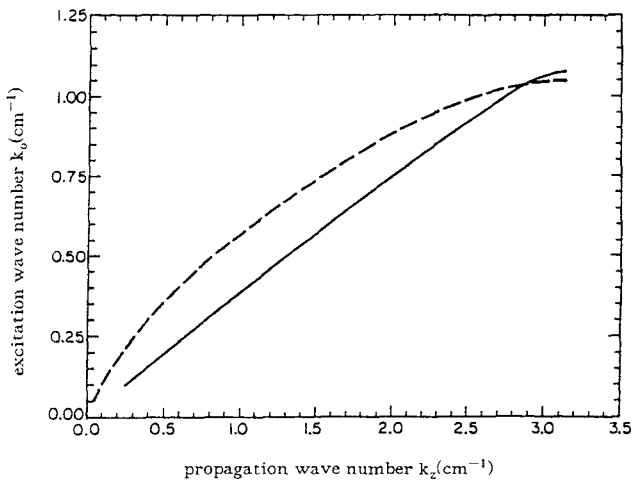

Fig. 11. Dispersion characteristics of the structure shown in Fig. 3. ---- balanced excitation; —— unbalanced excitation ($R_s = 0$, $w = 0.25$ cm, $a = b = 0.75$ cm, $d_1 = d_2 = 1.0$ cm, $N = 8$, $M = 16$, $\epsilon_{r1} = \epsilon_{r3} = 1$, $\epsilon_{r21} = 10$, $\epsilon_{r22} = 4$, $t_{21} = 0.4$ cm, $t_{22} = 0.1$ cm.)

wavenumbers for the balanced and unbalanced modes are higher than those shown in Fig. 9. We also note that more eigenvalues can be found for (37) for higher operating frequency after the balanced or unbalanced modes are cut off. These eigenvalues correspond to the higher order propagating modes and need further investigation.

Side-by-side coupling between two adjacent signal lines depicted in Fig. 6 has been studied and the results in terms of coupling length are tabulated in Table I. Good agreement with the results from Rubin and Bertoni [7] is obtained.

VI. Conclusions

The dispersion characteristics of parallel signal lines embedded in a multilayered structure in the presence of a periodically perforated ground plane have been analyzed. In this analysis, the spectral Green's function tensor is derived using the spectral-domain immitance approach in conjunction with the transfer matrix method to account for the multilayered medium. Rooftop basis functions and Galerkin testing procedures are employed, resulting in rapidly convergent, doubly infinite series for the eigenvalue problem which determines the propagation constant of the structure. It has been shown that the dispersion characteristics, as well as the cutoff wavenumbers, for both the balanced and unbalanced excitations of the signal lines strongly depend on the dielectric materials which support the signal lines and the perforated ground plane.

TABLE I
Normalized Coupling Length at $k_0 = 0.001$ cm

		k_z / k_0		$\Delta k_z / k_0$	l / λ_0
		even mode	odd mode		
(a)	Razor-blade testing [7]	1.0420	1.0039	0.0381	13 12
	Galerkin testing	1.0407	1.0040	0 0367	13 62
(b)		2.5544	2.3032	0.2512	1.99

Unit cell of Fig. 6 (a) In free space. (b) Signal lines and perforated ground plane are supported by two-layered dielectric as shown in Fig. 3. $\epsilon_{r1} = \epsilon_{r3} = 1$, $\epsilon_{r21} = 10$, $\epsilon_{r22} = 4$, $t_{21} = 0.4$ cm, and $t_{22} = 0.1$ cm.

References

[1] A. J. Blodgett, Jr., "Microelectronic packaging," *Sci. Amer.*, pp. 86–97, July 1983.
[2] T. Itoh and R. Mittra, "A technique for computing dispersion characteristics of shielded microstrip lines," *IEEE Trans. Microwave Theory Tech.*, vol. MTT-22, pp. 896–898, Oct. 1974.
[3] T. Itoh, "Analysis of microstrip resonators," *IEEE Trans. Microwave Theory Tech.*, vol. MTT-22, pp. 946–952, Nov. 1974.
[4] T. Itoh, "Spectral domain immitance approach for dispersion characteristics of generalized printed transmission lines," *IEEE Trans. Microwave Theory Tech.*, vol. MTT-28, pp. 733–736, July 1980.
[5] L. P. Schmidt and T. Itoh, "Spectral domain analysis of dominant and higher order modes in finline," *IEEE Trans. Microwave Theory Tech.*, vol. MTT-28, pp. 981–985, Sept. 1980.
[6] E. G. Farr, C. H. Chan, and R. Mittra, "A frequency-dependent coupled-mode analysis of multiconductor microstrip lines with application to VLSI interconnection problems," *IEEE Trans. Microwave Theory Tech.*, vol. MTT-34, pp. 307–310, Feb. 1986.
[7] B. J. Rubin and H. L. Bertoni, "Waves guided by conductive strips above a periodically perforated ground plane," *IEEE Trans. Microwave Theory Tech.*, vol. MTT-31, pp. 541–549, July 1983.
[8] B. J. Rubin, "The propagation characteristics of signal lines in a mesh-plane environment," *IEEE Trans. Microwave Theory Tech.*, vol. MTT-32, pp. 522–531, May 1984.
[9] C. H. Chan and R. Mittra, "On the analysis of frequency selective surfaces using subdomain basis functions," to be published in *IEEE Trans. Antennas Propagat.*
[10] P. M. van den Berg, W. J. Ghijsen, and A. Venema, "The electric-field problem of an interdigital transducer in a multilayered structure," *IEEE Trans. Microwave Theory Tech.*, vol. MTT-33, Feb. 1985.
[11] C. H. Chan and R. Mittra, "Analysis of MMIC structures using an efficient iterative approach," *IEEE Trans. Microwave Theory Tech.*, vol. 36, pp. 96–105, Jan. 1988.

Chi Hou Chan (S'86–M'87) was born in Macao on April 16, 1959. He attended Hong Kong Polytechnic and the City College of New York.

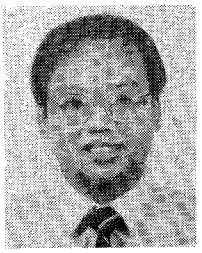

He received the B.S. and M.S. degrees in electrical engineering from the Ohio State University, Columbus, OH, in 1981 and 1982, respectively, and the Ph.D. degree in electrical engineering from the University of Illinois, Urbana, IL, in 1987.

From 1981 to 1982, he was a Graduate Research Associate at the ElectroScience Laboratory, Ohio State University. Since August 1982, he has been with the Electromagnetic Communication Laboratory in the Department of Electrical and Computer Engineering at the University of Illinois, where he is presently a Visiting Assistant Professor. His research interests include numerical techniques in electromagnetics, scattering from electrically large bodies, frequency-selective surfaces, microwave integrated circuits, high-speed digital circuits, and integrated optics.

Raj Mittra (S'54–M'57–SM'69–F'71) is the Director of the Electromagnetic Communication Laboratory of the Electrical and Computer Engineering Department and Research Professor of the Coordinated Science Laboratory at the University of Illinois. He is a Past-President of AP-S. He serves as a consultant to several industrial and governmental organizations in the United States.

His professional interests include the areas of analytical and computer-aided electromagnetics, high-speed digital circuits, radar scattering, satellite antennas, microwave and millimeter-wave integrated circuits, frequency-selective surfaces, EMP and EMC analysis, and interaction of electromagnetic waves with biological media.